Journal of Non-Crystalline Solids 379 (2013) 131–144

Non-stoichiometric crystallization of lithium metasilicate–calcium metasilicate glasses. Part 2 — Effect of the residual liquid

Vladimir M. Fokin [a,b,*], Raphael M.C.V. Reis [b], Alexander S. Abyzov [c], Clever R. Chinaglia [b], Jürn W.P. Schmelzer [d], Edgar D. Zanotto [b]

[a] Vavilov State Optical Institute, ul. Babushkina 36–1, 193 171, St. Petersburg, Russia
[b] Vitreous Materials Laboratory, Department of Materials Engineering, Federal University of São Carlos, UFSCar, 13565–905 São Carlos, SP, Brazil
[c] National Science Centre Kharkov Institute of Physics and Technology, Academician Street 1, 61108 Kharkov, Ukraine
[d] Institut für Physik, Universität Rostock, 18051 Rostock, Germany

ARTICLE INFO

Article history:
Received 10 June 2013
Received in revised form 31 July 2013
Available online 1 September 2013

Keywords:
Glass;
Crystallization;
Growth;
Eutectic;
Metastable liquidus

ABSTRACT

Crystallization of non-stoichiometric glasses of the $Li_2O \cdot SiO_2$–$CaO \cdot SiO_2$ joint (which has a simple eutectic) at deep undercooling proceeds in two stages. In the first stage, lithium metasilicate (LS) crystals are formed. In the second stage, after a considerable delay, it is supplemented by the evolution of a calcium metasilicate (CS) phase. The analysis of the evolution of the residual liquid composition and its effect on the crystallization process revealed a novel phenomenon. The formation of LS crystals in the first stage of the process leads to the establishment of a temporary equilibrium between the residual liquid and the LS-crystal phase. As a result, LS crystal growth is temporarily arrested. This termination of LS crystal growth occurs when the composition of the residual liquid reaches that of the metastable *liquidus* for LS at given temperature and pressure. The growth of LS crystals is resumed only in the second stage of the process when the CS crystals form. The evolution of the CS-crystal phase changes the composition of the residual liquid and shifts it away from the composition corresponding to the metastable *liquidus*. As the result, the LS crystals again become capable of further growth. The above crystallization pathway is expected to be a general phenomenon in phase formation in multi-component systems with different mobilities of the components determining the kinetics of formation of the different phases.

1. Introduction

Crystallization of non-stoichiometric glass-forming liquids (i.e. liquids with compositions different from that of the precipitating crystalline phases) is a quite common phenomenon in glass–ceramics technology. Hence, the study of these liquids is of considerable practical interest (see for example [1–4]). Moreover, the investigation of the crystallization of non-stoichiometric liquids may supply us with additional experimental data for testing and further advancement of phase transition theories for multi-component systems.

In general, the different crystalline phases that may precipitate in a given non-stoichiometric system will have quite different nucleation and growth rates. As a rule, the formation of such phases results in local and eventually global changes of the composition of the residual liquid in the advanced stages of phase transformation when the volume fraction of the crystalline phases has become sufficiently large. Changes in the composition of the ambient phase (depletion effects) may quantitatively and qualitatively affect the nucleation-growth kinetics and the overall course of the phase transformation process [5–7]. In the present paper, results of experimental measurements of phase formation in such non-stoichiometric systems and their analysis are outlined. Particular attention is directed hereby to the analysis of the evolution of the composition of the residual liquid and its effect on the crystallization kinetics. It is believed that the results are of relevance not only for the particular system studied but represent a typical general feature of phase formation in multicomponent, non-stoichiometric glass-forming melts.

In the present paper, we focus the attention on glass-forming systems with compositions belonging to the $Li_2O \cdot SiO_2$–$CaO \cdot SiO_2$ joint, which has a simple eutectic. Since all the different non-stoichiometric glass compositions of this joint crystallize into only two stable phases (lithium metasilicate, LS, and calcium metasilicate, CS), this system may serve as a simple model for investigating the kinetics of simultaneous formation of multiple crystalline phases in the same undercooled glass-forming liquid. We continue here the analysis performed in our previous study [8]. There our attention was directed to the *initial* stages of crystallization, i.e. to the stage of the process with small (<10%) volume fractions of the evolving crystal phases. Under such conditions, the effect of the evolution of the residual liquid composition on crystallization could be neglected, at least, to a reasonable approximation. We

* Corresponding author at: Vavilov State Optical Institute, ul. Babushkina 36–1, 193 171, St. Petersburg, Russia. Tel.: +7 812 355 30 38.
E-mail address: vmfokin@gmail.com (V.M. Fokin).

0022-3093/$ – see front matter © 2013 Elsevier B.V. All rights reserved.
http://dx.doi.org/10.1016/j.jnoncrysol.2013.08.006

showed that, in glasses with compositions between lithium metasilicate and the eutectic and at temperatures close to the glass transition temperature (T_g), LS is the primary evolving phase. In particular, it was also demonstrated that the bulk nucleation rates in these glasses strongly increase with the increasing Li_2O content of the initial glass-forming melt, whereas the crystal growth rates increase only weakly. Continuing the analysis of [8], the present paper addresses the *advanced* stages of crystallization including, in addition to the analysis of the initial precipitation of lithium metasilicate, the study of the subsequent precipitation of calcium metasilicate crystals. In this analysis, we focus primarily onto studying the evolution of the residual liquid composition and its effect on the overall crystallization process. It will be shown, in particular, that the preferential formation initially of only LS-crystals and their growth leads to the establishment of a temporary metastable equilibrium state between LS-crystals and the melt inhibiting the further growth of the LS-crystals. The growth is renewed only after formation of CS-crystals and the resulting from this process changes of the composition of the residual liquid.

The paper is structured as follows. In Section 2, we briefly describe materials and methods of analysis employed. In Section 3, results of the growth kinetics of crystals nucleated on the surface and in the bulk of the glass samples are presented and analyzed. In Section 4, the existence of diffusion zones around the growing crystals is demonstrated. Finally, a general discussion of the results and further possible developments (Section 5) completes the paper.

2. Materials and methods

In the present study we investigated glass-forming compositions belonging to the $Li_2O \cdot SiO_2$–$CaO \cdot SiO_2$ joint. The glasses were prepared from lithium (Alfa Aesar) and calcium (Sigma-Aldrich) carbonates and fumed silica (Aldrich). Solid-phase reactions of the desired mixtures of these reagents were carried out at 800–900 °C in about 48 h. The calcined material was then melted at 1400 °C for 4 h in a platinum crucible employing an electrical furnace. The melts were poured onto a steel (or brass) slab and pressed by a steel (or brass) plate.

The compositions of the glass-forming melts studied in the present investigation are marked on the phase diagram (Fig. 1) by the letter B, with subscripts corresponding to the nominal content of CS in mol%. This notation is used throughout the paper. The standard methods of analysis of the initial and crystallized glasses are described in detail in ref. [8]. For the optical analysis of crystallized glasses and DSC analysis we employed small cubic glass samples. First plane-parallel plates were prepared from the parent glass and then they were cut by a diamond disk.

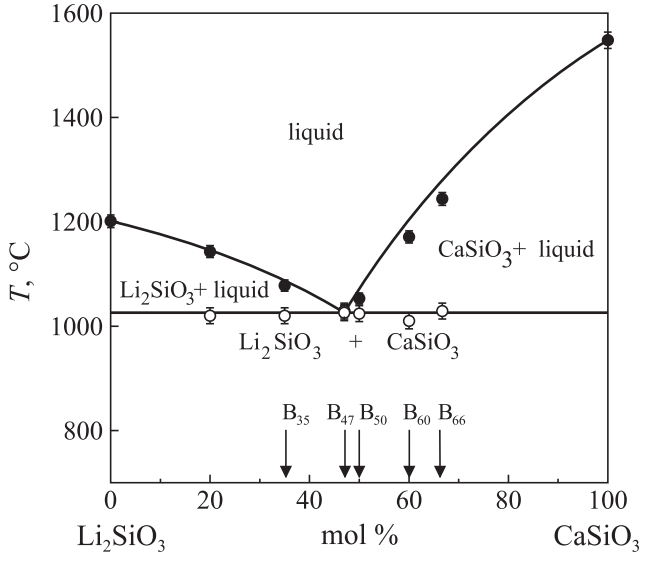

Fig. 1. Phase diagram of the pseudo-binary joint Li_2SiO_3 – $CaSiO_3$. Lines are taken from [9]. Points are data estimated from DSC curves [8]. Glass compositions employed in the present study are marked by arrows. Subscripts of letter B correspond to the $CaO \cdot SiO_2$ content in the glasses.

3. Growth of lithium disilicate crystals formed by surface and bulk nucleation

As we have shown in [8], without preliminary nucleation treatment glasses with compositions close to the eutectic (B_{50}, B_{47}) crystallize from the sample surface only. On the other hand, glass B_{35} reveals extremely high bulk nucleation rates of LS crystals. The number of LS-nuclei formed in the glass B_{35} (both during melt quenching in glass preparation and during heating to the studied temperature) is very high, approximately equal to $N_0 \approx 10^6$ mm^{-3}. Therefore, we will separately examine the surface crystallization of glasses B_{50} and B_{47} and of bulk crystallization of glasses B_{50}, B_{47} and B_{35}.

3.1. Surface crystallization

Fig. 2a shows DSC (differential scanning calorimeter) scans with a heating rate of 10 °C/min for B_{47} cubic glass samples with edge lengths of approximately 2 mm. The samples were previously heat-treated in a tube furnace at $T = 675$ °C for different periods of time. Two crystallization peaks can be identified. The first one is caused by the crystallization of LS, and the second one results from the crystallization of both LS and CS. As the isothermal heat-treatment time t increases, the area of the first peak is reduced, with little or no influence on the second crystallization peak. This process proceeds for approximately 7 min. Fig. 2b shows the glass transition temperature range of the DSC scans. The temperature of the onset of the glass transition, T_g, for the as-cast sample ($t = 0$ min) is 475 °C. Increasing the previous heat-treatment times at 675 °C has little effect on T_g, although the intensity of the transition diminishes due to the partial crystallization of the glass. Interestingly, a second glass transition temperature can be detected for $t > 5$ min. Temperatures and intensities increase with treatment time. Hereinafter, all values of T_g relate to glass transition temperatures measured by the DSC method.

An optical micrograph of a polished cross section of a sample heat-treated for 5 min at 675 °C is shown in Fig. 3a. The microstructure reveals a surface layer consisting of LS crystals with residual glass in between them. An SEM BSE (back scattered electrons) image of the same sample is shown in Fig. 3c and d. The residual glass between the growing LS crystals is of a lighter color than the glass in the central part. Only lithium and calcium metasilicates were detected by XRD (X-ray diffraction) in the studied glasses [8]. For this reason, the Si-concentration should be approximately constant throughout the sample. As BSE reveals chemical contrast, one can infer that the glass between the LS crystals contains more Ca than does the liquid in the sample center. The presence of two distinct glasses in the samples is corroborated by the observation of two glass transition temperatures in the DSC-curves of Fig. 2b for the partially crystallized cubic samples.

The sample includes two types of residual glasses with rather different compositions. Therefore, the chemical stability of the Ca-rich melt in the surface layer (containing approximately 65-75 mol% CS) is expected to be higher than that of the melt in the center, where the composition is close to the composition of the parent glass (47 mol% CS). This conclusion is confirmed by Fig. 3b and e, which show reflected light-optical micrographs of the same cross section of the sample taken after a time interval of two months. With the lapse of time, the glass in the sample center changes due to interaction with the atmosphere, while the surface layer is practically unaltered (Fig. 3b).

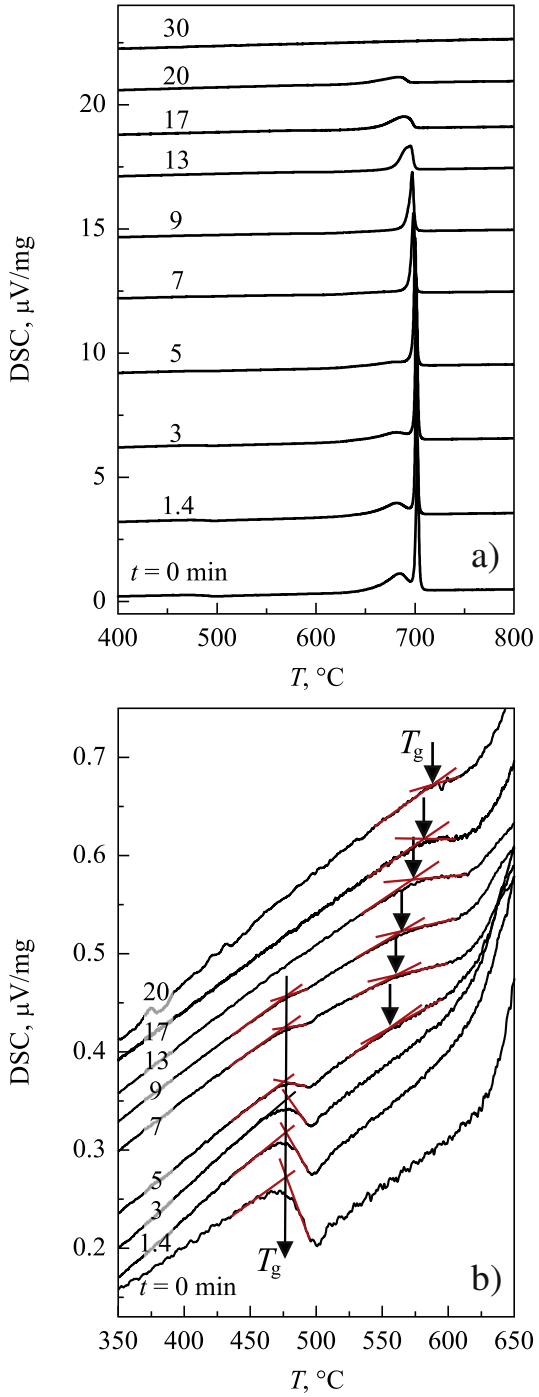

Fig. 2. DSC heating scans with a rate of 10 °C/min for B_{47} cubic glass samples, with edge of about 2 mm. The samples were previously heat-treated in a tube furnace at $T = 675$ °C for different times t noted close to proper curves. a) Large temperature range including crystallization peaks. b) Smaller temperature range including the glass transition temperatures.

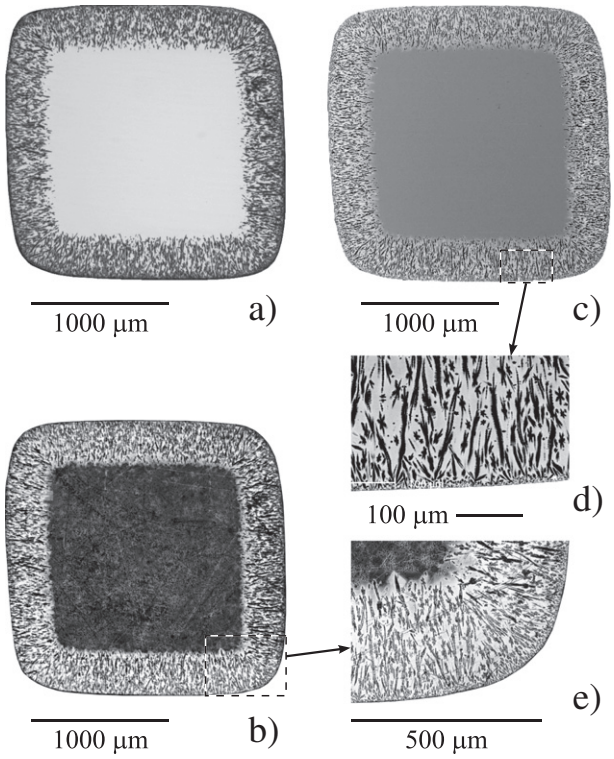

Fig. 3. Reflected light optical micrographs (a, b, e) and SEM BSE images (c, d) of the cross section of cubic shaped sample of glass B_{47} heat-treated at $T = 675$ °C for 5 min. The micrographs (a, fresh) and (b, old) were performed within an interval of 2 months.

Fig. 4 shows data related to B_{47} cubic glass samples that were heat-treated for different periods of time at $T = 675$ °C. The thickness of the surface layer (including LS crystals and the residual melt) was measured as a function of time (see Fig. 4a). Fig. 4b shows the volume fraction of the surface layer calculated from the data given in Fig. 4a. The glass transition temperatures T_g for both residual glasses (Fig. 2b) are shown in Fig. 4c. Using the dependence of the glass transition temperature on the composition of glasses belonging to the LS–CS joint (see Fig. 3 in [8]) and assuming that the residual glasses are homogeneous, we estimated the compositions of the residual glasses in the partially crystallized sample (see Fig. 4d). The results obtained by this simple method were confirmed by results of EDS measurements shown below. In contrast to the behavior in the sample center, the composition of the liquid between the oriented crystals in the surface layer, and hence its glass transition temperature, slowly changes with heat-treatment time (Fig. 4c and d).

The composition of the residual glass, estimated via its glass transition temperature, is only an average value and does not appropriately reflect the existing composition gradients in the diffusion zones. This topic will be discussed in more detail in Section 4. According to Fig. 4d, at $T = 675$ °C and in the course of at least $t \sim 8$ min, the melt composition of the sample center does not change appreciably. Moreover, the interface between the melt in the central part of the cubic sample and the partially crystallized surface layer can be considered to a first approximation to be planar, thus the size of the diffusion zone does not depend on the thickness of the surface layer. The above properties result in a time-independent crystal growth rate in the direction perpendicular to the external surface of the sample (see Fig. 4a). Starting at $t \sim 8$–10 min, the dependence of layer thickness h on time t begins to deviate from a linear one. However, by this time, the volume fraction of the central part does not exceed 10% of the total sample volume (Fig. 4b). Consequently, we can suppose that the liquid in the central part no longer retains the initial glass composition. A prolongation of heat-treatment time at $T = 675$ °C from 20 to 30 minutes results in full crystallization, which is confirmed by the lack of any thermal effect on the DSC heating curve (see Fig. 2a). An example of fully crystallized B_{47} glass is shown in Fig. 5.

As shown in Fig. 4c, the glass transition temperature of the glassy part of the surface layer is much higher than that of the internal part of the sample. This difference results in tensile stresses. In Fig. 6, residual

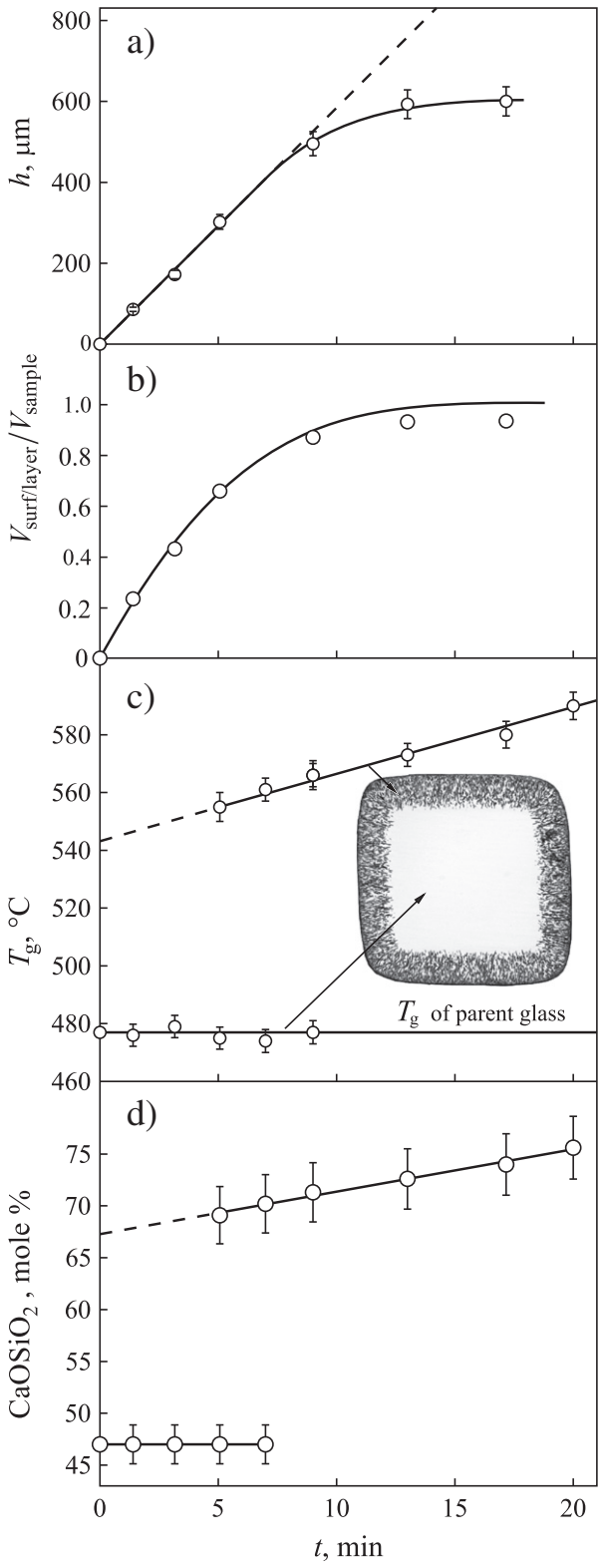

Fig. 4. Dependences of the different parameters of the B_{47} glass sample shaped as cube with an edge length of 2 mm on heat-treatment time at $T = 675$ °C: thickness (a); reduced volume of surface layer (b); glass transition temperatures (c); and compositions (d) of residual glass in surface layer and melt in the internal part of the sample. Line in (a) is a guide to the eye, (b) is calculated for the case of a time-independent growth rate of crystalline layer thickness, (c) and (d) are linear fits.

stresses in the glassy center of the sample are revealed by cross-polarized transmitted light microscopy. These stresses arise in the course of cooling to room temperature because the surface layer

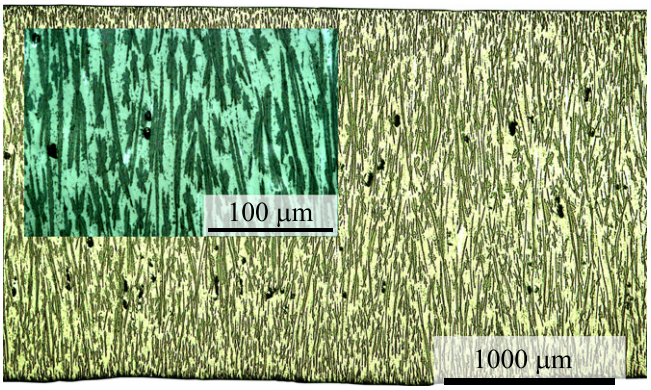

Fig. 5. Optical photograph of the orthogonal cross section of the plane-parallel plate of B_{47} glass fully crystallized at 675 °C for 30 min. Light and dark parts correspond to CS and LS crystals, respectively.

undergoes the glass transition earlier than the bulk part of the sample. For this reason, the surface layer acts as a solid cage boundary during subsequent cooling, resulting in stresses.

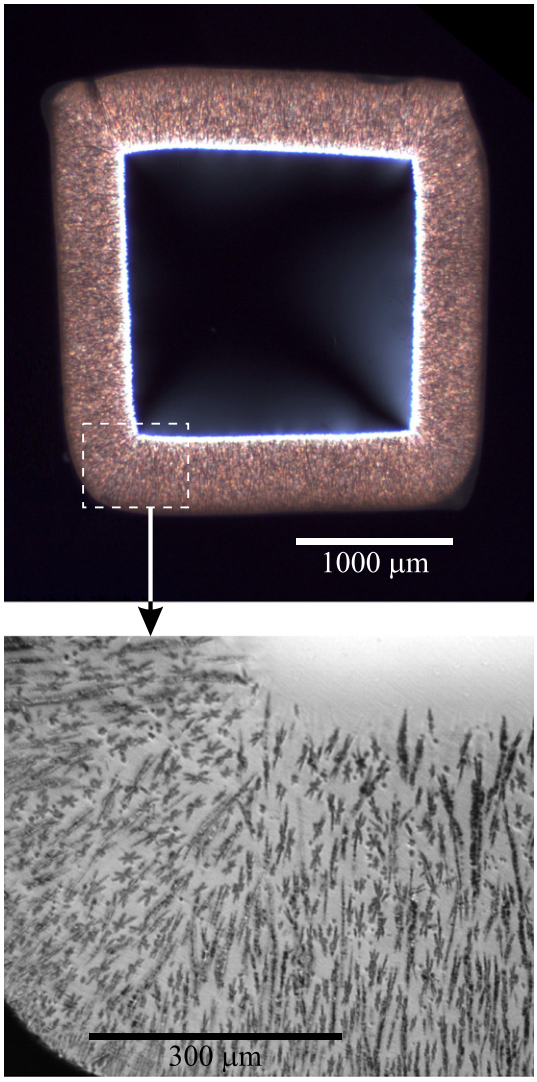

Fig. 6. Micrographs of glass B_{47} sample with regular shape heat-treated at 675 °C for 5 min. To take the photographs two parallel faces were removed. Top image is received by cross-polarized transmitted light microscopy and bottom — by reflected light microscopy.

3.2. Bulk crystallization

3.2.1. Glass B_{47}

To promote the formation of LS crystals in the bulk of the B_{47} glass, a preliminary nucleation treatment was performed at a temperature $T_n = 470$ °C for different periods of time. Fig. 7a shows DSC-curves of glasses nucleated for $t = 0$, 4.5, 19, and 45 hours. The nucleation treatments resulted in a strong shift of the first exothermic peak (related to the crystallization of LS) to lower temperatures, while only a subtle temperature change was observed for the second peak. This shift is shown in Fig. 7b, which presents the temperatures for the maxima of both crystallization peaks. The temperature of the first crystallization peak decreases with nucleation time, as higher numbers of LS crystals result in faster overall crystallization kinetics; hence, the release of the heat of crystallization can be detected at a lower temperature [10]. As will be shown below, the second peak is stimulated by heterogeneous nucleation of CS and reflects the simultaneous crystallization of CS and LS. However, as the kinetics of CS crystallization is strongly limited by the relatively low mobility of Ca (compared to that of Li), the influence of increasing temperature is much stronger as compared to the effect of the increase of LS crystal number. This argument explains the weak influence of the preliminary nucleation step on the temperature of the second peak.

Another DSC experiment on preliminary overall crystallization was performed to study how its kinetics is affected by the evolution of the residual melt composition. To promote the formation of LS crystals in the B_{47} glass volume, a preliminary nucleation treatment was performed at a temperature $T_n = 470$ °C for 45 h. After this treatment, the crystal number density N reached a value of approximately 10^4 mm^{-3}. Small pieces of this sample were then heat-treated at $T_d = 675$ °C for different periods of time and afterward analyzed by DSC, optical microscopy, SEM, and EDS. DSC heating curves of such preliminarily heat-treated bulk samples are shown in Fig. 8. The evolution of the glass transition temperature of the residual liquid and its composition (estimated via T_g as described in Section 3.1) is shown in Fig. 9a and b, respectively. The Ca content calculated from EDS measurements is also included in Fig. 9b. For this analysis, a parent glass with known (nominal) composition was employed as the standard sample. The two different methods yield similar results.

Fig. 10 shows a reflected light optical micrograph and an SEM SE image of a cross section of a B_{47} glass sample heat-treated at $T_n = 470$ °C for 45 h and then at $T_d = 675$ °C for $t = 2.5$ min. The dark rectangles in the SEM SE image marked by arrows show the location of the EDS measurements.

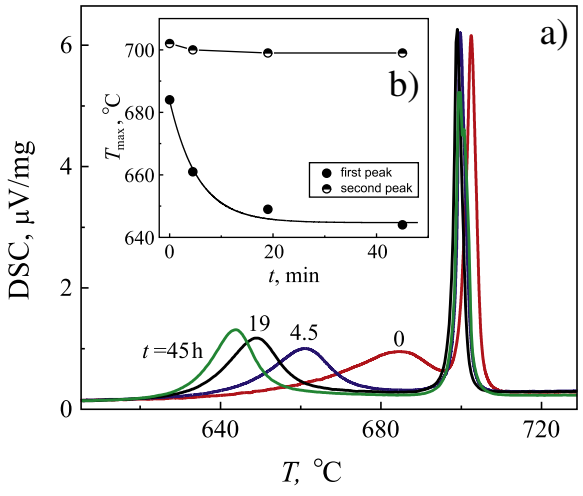

Fig. 7. DSC heating curves of B_{47} glass preliminary heat-treated at nucleation temperature $T_n = 470$ °C for different times as denoted close to proper curves. Inset shows the position of the first and second exothermic peaks *versus* nucleation time.

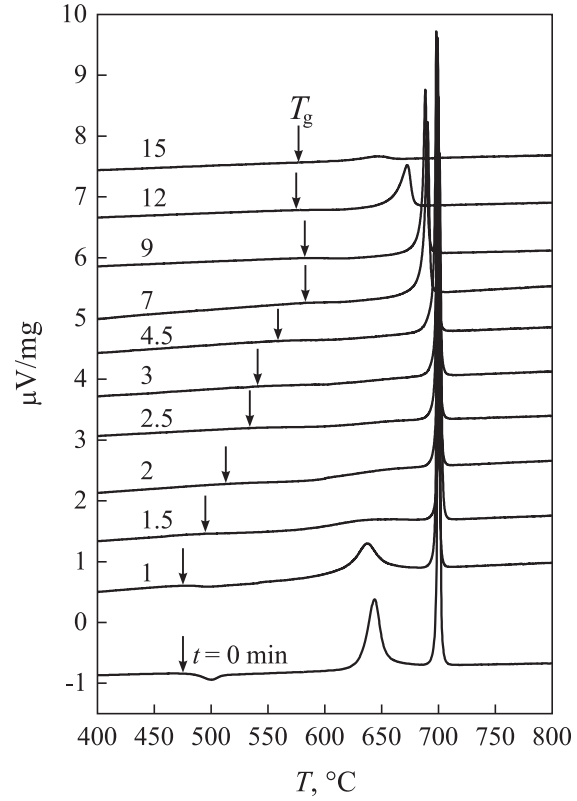

Fig. 8. DSC heating curves (10 K/min) of B_{47} glass bulk samples subjected to nucleation heat-treatment at $T = 470$ °C for 45 h followed by heat-treatment at $T = 675$ °C for different periods of time t indicated at the respective curves.

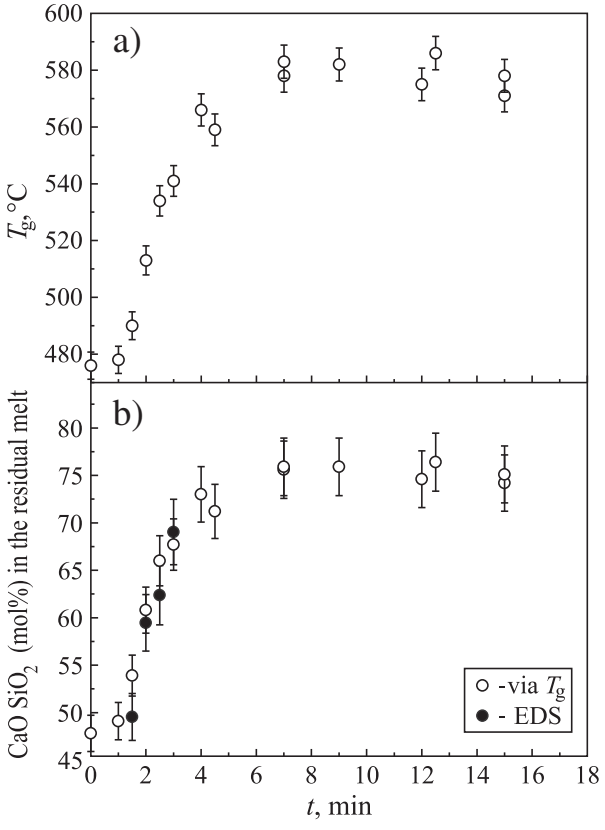

Fig. 9. Evolution of (a) the glass transition temperature of the residual melt and (b) its composition (estimated by two different methods) during bulk crystallization of the B_{47} glass at $T = 675$ °C.

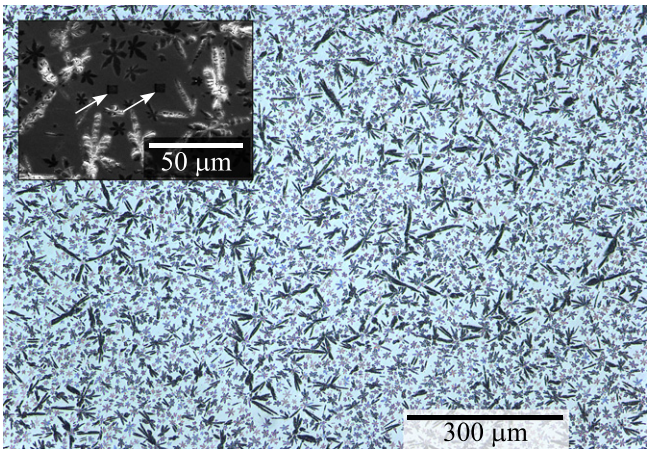

Fig. 10. Reflected light-optical micrograph and SEM SE image (inset) of the cross section of B_{47} glass sample heat-treated at T_n = 470 °C for 45 h and then at T_d = 675 °C for 2.5 min. Arrows in the inset image mark the places of EDS measurements.

Expressing the content of LS in percent in the residual, $X_{LS}^{r/l}$, and in the parent liquid, $X_{LS}^{p/l}$, and neglecting the small difference between the densities of the glassy and crystalline phases, we can write the following equation for the crystal volume fraction, α:

$$\alpha = \frac{X_{LS}^{p/l} - X_{LS}^{r/l}}{100 - X_{LS}^{r/l}}. \quad (1)$$

Based on the data for the residual melt composition (Fig. 9b), we employed Eq. (1) to estimate the volume fraction of LS crystals. The dependence of overall crystallization on time is shown in Fig. 11a and b in normal and Avrami [ln(−ln(1 − α)) *versus* ln(*t*)] coordinates, respectively. According to Fig. 11b, in the initial stages of the phase transition ($t \le 2$ min), the value of the Avrami parameter *n* in Eq. (2),

$$\alpha(t) = 1 - \exp(-Pt^n), \quad (2)$$

proposed in [11] for describing overall crystallization, is close to 3. In our case, the nucleation rate at T_d = 675 °C can be neglected, and the crystal number density *N* is constant ($N \sim 10000$ mm^{-3}). Consequently, the value $n = 3$ corresponds to crystal growth with a constant rate. With a further advancement of the process, the crystal growth rate strongly decreases and, at $t \sim 7$ min, the growth practically stops. This termination of LS crystal growth is not caused by the full exhaustion of lithium in the residual melt because it still contains approximately 25 mol% LS (see Fig. 9b). By this reason, another explanation has to be searched for and will be developed below.

The above method for estimating the crystal volume fraction via the composition of the residual glass is valid if only one crystalline phase forms. Hence, this method is restricted to the time period before CS crystals appear. The overall evolution of the crystallization of LS and CS can be qualitatively analyzed using the areas of the crystallization peaks from DSC curves. Fig. 12a presents the areas of the first (A_1, crystallization of LS crystals) and second peaks (A_2, simultaneous crystallization of CS and LS crystals from the residual liquid) of the DSC curves shown in Fig. 8 *versus* crystallization time *t* at T_d = 675 °C. At $t = 0$ the total area A^0_{total} of the exothermic peaks corresponds to full crystallization of the entire sample in the DSC (the volume of crystals already nucleated at T_n = 470 °C can be neglected). Due to the preliminary growth of crystals at T_d = 675 °C, the total area A^t_{total} decreases and approaches zero at t = 17–20 min, indicating that full crystallization was reached. Thus, the difference Δ*A* between A^0_{total} and A^t_{total} shown in Fig. 12b is qualitatively related to the volume fraction of the crystalline phases formed prior to the DSC analysis. The evolution of this

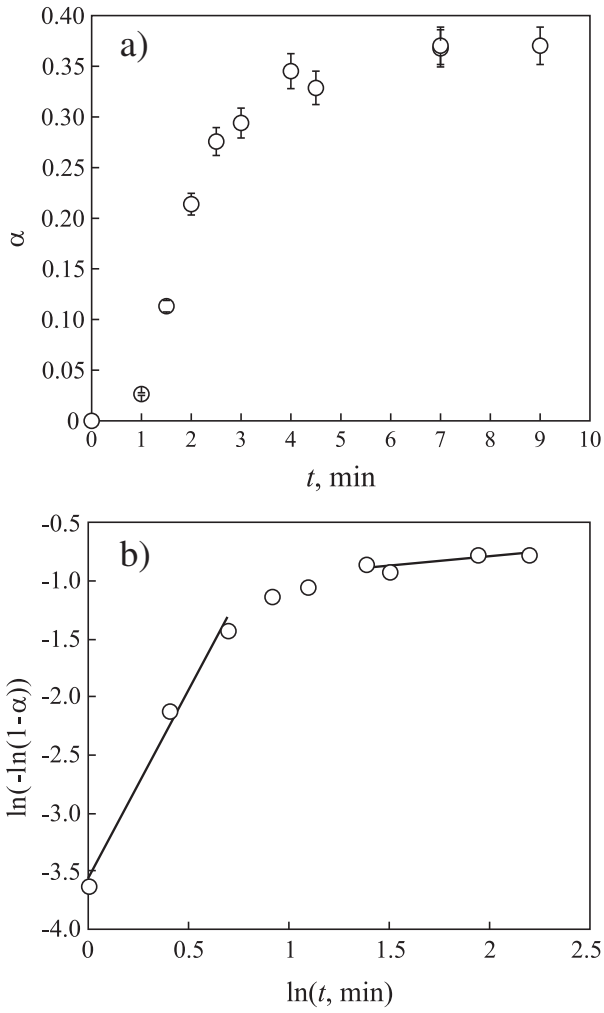

Fig. 11. Volume fraction of LS crystals as a function of heat-treatment time at T = 675 °C after nucleation at T = 470 °C for 45 h in (a) normal and (b) Avrami coordinates. Solid lines are linear fits.

difference reflects the kinetics of overall crystallization. Crystallization proceeds in two well-separated stages. The crystallized volume in the initial stage of phase transformation first increases for a time $t \sim 3$–4 min, corroborating the result shown in Fig. 11. The crystallization is then arrested until a time of $t \sim 7$–8 min is reached, when it recommences and finally results in full crystallization. The composition of the residual liquid notably reaches approximately 75 mol% CS and does not change further after $t \sim 4$–5 min (see Fig. 9b). This feature is of special interest, as it suggests the simultaneous crystallization of two phases at times $t > 8$ min, resembling, as will be shown below, the high temperature crystallization of a glass with eutectic composition. Please recall that, in the case of surface crystallization, the composition of the residual melt in the surface layer between LS crystals (see Fig. 4d) is close to that for volume crystallization.

Thus, the two-stage behavior of overall crystallization occurs for the following reasons: i) fast crystallization of lithium metasilicate accompanied by a shift of the residual liquid composition towards increased calcium metasilicate content; ii) slowing down and temporary termination of LS growth when the residual liquid reaches a particular composition; and iii) heterogeneous nucleation of CS crystals after a relatively extended induction period, resulting in the formation of diffusion zones enriched by lithium and the resumption of LS growth, however, in this case, together with CS similar to eutectic crystallization. The above sequence of crystalline phase formation at constant temperature, but

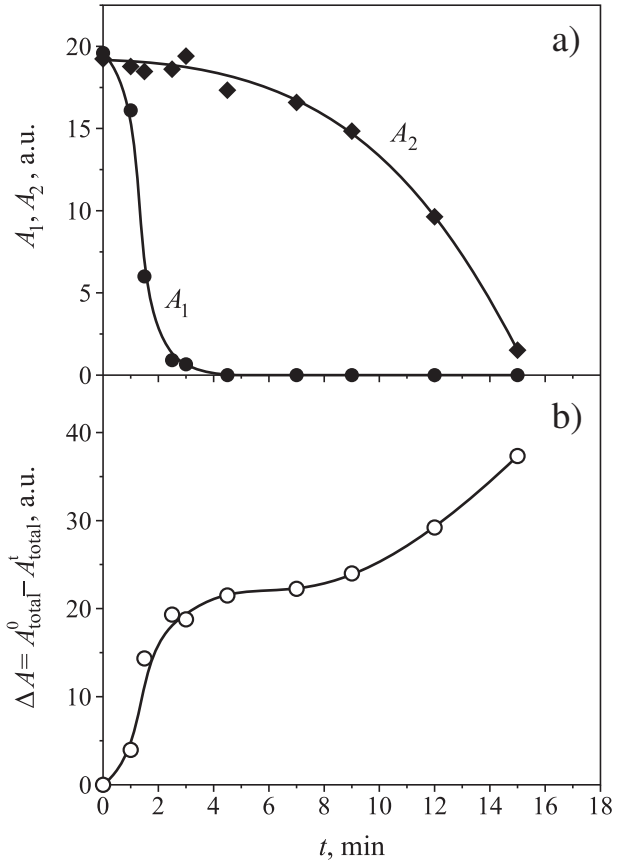

Fig. 12. Time-dependencies of preliminary crystallization of the B_{47} glass at $T = 675$ °C: a) areas of the first and second crystallization peaks on DSC curves (see Fig. 8); b) difference between the total area crystallization (peak 1 plus peak 2) of the sample subjected only to nucleation heat-treatment ($t = 0$) and that of the preliminary partly crystallized samples.

with changing composition, was corroborated by the XRD-measurements shown in Fig. 13. This analysis detected only LS crystals in samples crystallized for $t = 4$ and 7 min, whereas, in a sample heat-treated for 12.5, 15 and 17 min, two phases were detected, LS and CS.

The decreased rate and subsequent arrest of LS formation, shown above for isothermal crystallization, is also found in a dynamic (heating) regime. Fig. 14 shows data obtained in a DSC experiment for B_{47} glass nucleated at $T_n = 470$ °C for 45 h. The heating curve (*a*) shows the two separate crystallization peaks for LS and LS + CS from the residual

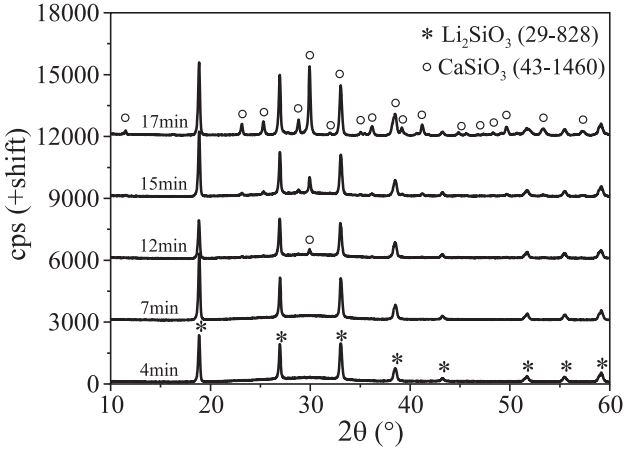

Fig. 13. XRD-spectra of B_{47} glass samples nucleated at $T = 470$ °C for 45 h and then crystallized at $T = 675$ °C for different periods of time given close to the respective spectra.

glass. The heating (*1*) and cooling (*2*) curves marked by (*b*) were obtained for a similar sample as in (*a*), but the heating run (*1*) was stopped at $T = 685$ °C, just after the end of the first exothermic peak, that is, after the crystallization of LS. A second heating run (*3*) up to $T = 800$ °C was performed for the same sample after cooling (*2*), revealing a strong increase in the glass transition temperature of the residual liquid due to the transfer of a significant amount of Li from the liquid to the crystalline phase (LS). In contrast to curves (*a*), curve (b) (*3*) reveals only one exothermic peak, corresponding to simultaneous crystallization of CS and LS from the residual melt.

According to the measured value of the glass transition temperature ($T_g = 589$ °C), after the first crystallization peak has evolved the residual liquid has the average composition 75CS25LS (mol%), that corresponds to the right side of the phase diagram (see Fig. 1). Note that the composition of the residual liquid in the non-isothermal DSC experiment coincides with the one achieved at the moment of arrest of LS crystallization in the isothermal experiment (Fig. 9). Thus, we can conclude that the sequence of phase formation in the dynamic regime, including the arrest of LS crystallization after the first exothermic peak, is similar to that at constant temperature; the only difference is that, after the arrest of LS crystallization, the formation of CS depends not only on time but also on temperature.

3.2.2. Glass B_{35}

In contrast to glass B_{47}, preliminary nucleation is not required for glass B_{35} to initiate bulk crystallization. This difference is due to the extremely high bulk nucleation rate of LS in glass B_{35}, resulting in a crystal number density of approximately $N_0 \approx 10^6$ mm^{-3} after the completion of sample preparation (as compared with $N_0 \sim 1$ mm^{-3} for glass B_{47}). In this case, the ratio between the number densities for both cases is close to that between the steady-state nucleation rates (see Fig. 11 in [8]). This result can be expected; at similar cooling and heating rates used for glasses B_{35} and B_{47}, N_0 should be proportional to the maximum nucleation rate.

Fig. 15 shows the radii, *R*, of LS spherulites *versus* heat-treatment time at a constant temperature $T = 560$ °C measured with optical microscopy. The dependence of *R* on *t* could be divided into two parts: an initial linear part (*1*), with a growth rate $U = 5.5 \cdot 10^{-9}$ m/s, and an advanced part (*2*) that could be approximately described by $R \sim t^{(0.55 \pm 0.03)}$ (see also Fig. 15 inset). This result allows us to suppose

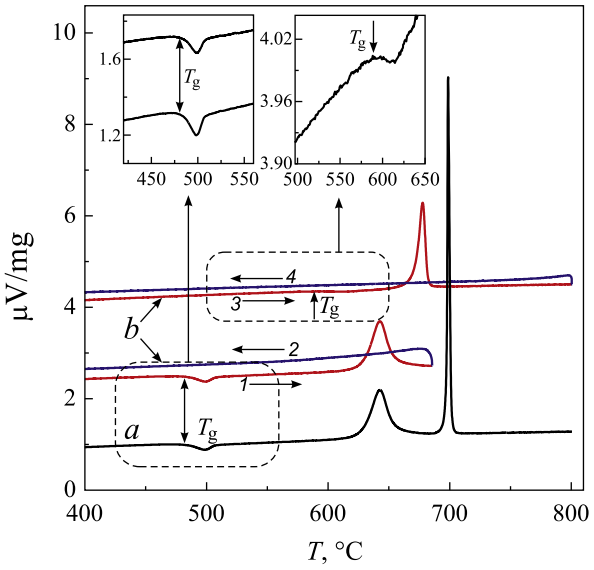

Fig. 14. DSC curves (10 K/min) of B_{47} glass. a) glass preliminary subjected to nucleation heat-treatment at $T_n = 470$ °C for 45 h; b) glass preliminary subjected to nucleation heat-treatment at $T_n = 470$ °C for 45 h: 1 — heating up to 685 °C, 2 — cooling down to 305 °C, 3 — heating up to 800 °C, and 4 — cooling down to room temperature.

that the growth in the initial stage is kinetically limited by processes occurring at the crystal/melt interface and switching later to a process of growth governed by the diffusion of Li through the diffusion zone forming around the crystals.

The above described dependencies are in good agreement with an analysis of the kinetics of overall crystallization performed based on Eq. (2). Fig. 16 shows (*a*) the original plot of the dependence of volume percentage of LS crystals on time (estimated both by light-optical microscopy and via the glass transition temperature T_g of the residual glass) and (*b*) the same data in coordinates $\ln(-\ln(1-\alpha))$ and $\ln(t)$ to estimate the Avrami coefficient n in Eq. (2), as indicated in the plot. The Avrami coefficient can be written as

$$n = k + 3m, \tag{3}$$

where k and m are obtained from the relations $N \sim t^k$ and $R \sim t^m$.

With the values of n and m, one can estimate the value of k using Eq. (3). The value of the parameter k is in our case close to zero, which corresponds to a constant number of growing crystals. That such result is indeed to be expected for the considered case is evident from the fact that the temperature $T = 560$ °C is about one hundred degrees higher than the temperature of the maximum nucleation rate. Therefore, here we deal mainly with nuclei nucleated prior to heat-treatment at $T = 560$ °C. For the case of a constant number of spherical crystals N_0, the coefficient P in Eq. (2) can be written as

$$P = \frac{4\pi}{3} N_0 U^3. \tag{4}$$

For glass B_{35}, the number N_0 of nuclei is approximately equal to $8.35 \cdot 10^5$ mm^{-3}. Taking the value of P (being equal to -9.4066 s^{-n}) from the linear fit of the first part of the Avrami plot (Fig. 16b), we estimated the growth rate to be equal to $U = 4.8 \cdot 10^{-9}$ m/s. This value is very close to the experimental one; compare the line (3) in Fig. 15, $R = U \cdot t$, with the linear fit (1) of the experimental data.

The growth of LS crystals is accompanied by a change in the residual melt composition and, hence, its glass transition temperature, as was previously demonstrated for glass B_{47}. Fig. 17a presents the DSC heating curves of the parent glass and the glass samples after heat-treatment at $T = 560$ °C for 10, 20, and 30 min. The evolution of the glass transition temperature and residual melt composition is shown in Fig. 17b. At a heat-treatment time of 30 min, the composition of the residual melt approaches that of glass B_{50}. Using the composition of the residual melt,

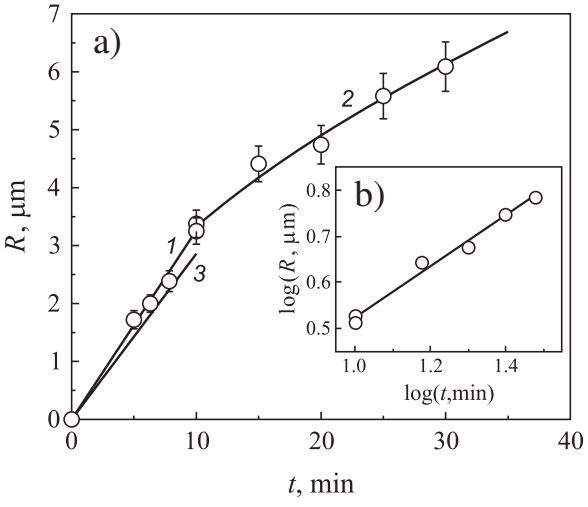

Fig. 15. a) Radius of LS-spherulites in B_{35} glass versus heat-treatment time at $T = 560$ °C. Line *1* is a linear fit and line *2* is plotted employing the relation $R = 0.95\ t^{0.55}$ corresponding to the linear (in a logarithmic scale) approximation shown in inset (b). Line *3* corresponds to the linear crystal growth rate estimated via Eq. (4) (see text).

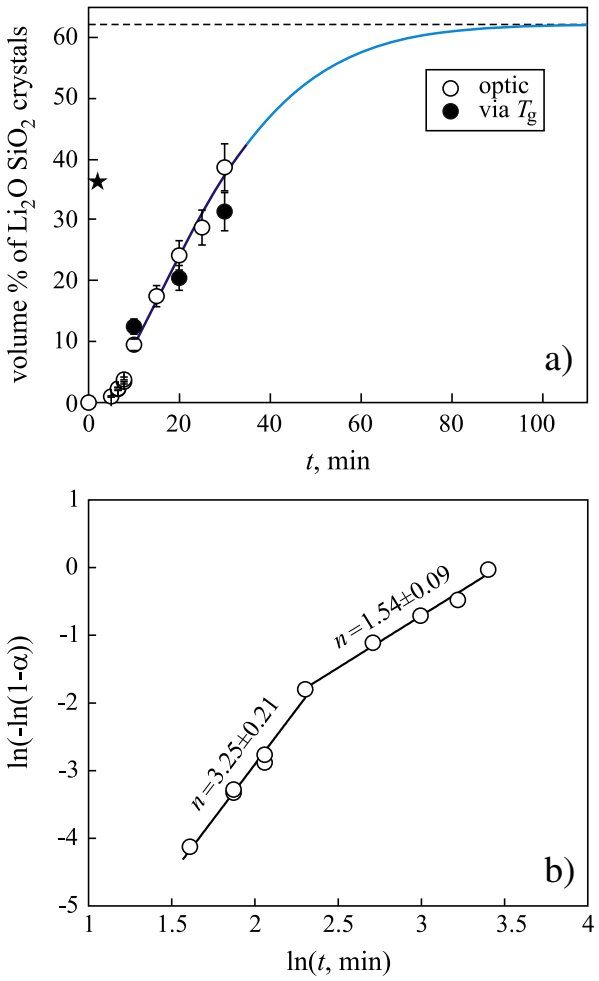

Fig. 16. Volume percent of LS crystals in the glass B_{35} *versus* heat-treatment time at $T = 560$ °C; solid line in (a) is plotted employing Eq. (2). It corresponds to the Avrami plot (b) where solid lines are linear fits.

we estimated the volume fraction of the crystalline phase from Eq. (1). These results are shown in Fig. 16a; they are nearly equal to those obtained with optical microscopy. The star in Fig. 16a (estimated via the value of the glass transition temperature T_g of the residual glass) refers to a glass sample subjected to preliminary nucleation at $T = 470$ °C for 12 h that strongly accelerates the kinetics of overall crystallization. It is more difficult to perform the analysis of growth and overall crystallization kinetics for lower temperatures because in such cases one has to account for the nucleation process during at least the initial stage of phase transformation.

Fig. 18 shows the DSC heating curves of B_{35} glass samples subjected to preliminary heat-treatment at $T = 520$ °C for different periods of time. Fig. 19 presents the dependences of different characteristic parameters of the system on the length of this time interval: LS crystal size (a), glass transition temperature (b), taken from DSC curves shown in Fig. 18, the residual glass composition, estimated via T_g (c), and the volume percent of the crystalline phase (d), estimated via the residual melt composition and optical microscopy.

Despite the lack of experimental data for the very early stage of crystallization, the Avrami parameter likely decreases from 4 to 3 over this time interval. This assumption agrees with the data given in the inset of Fig. 19d, showing the overall crystallization kinetics. Thus, it is reasonable to assume that for the time up to $t \sim 80$–100 min, the overall crystallization proceeds via simultaneous nucleation and growth processes. Afterwards the nucleation rate strongly decreases and tends to zero, due to the change in the residual melt composition. Indeed, close

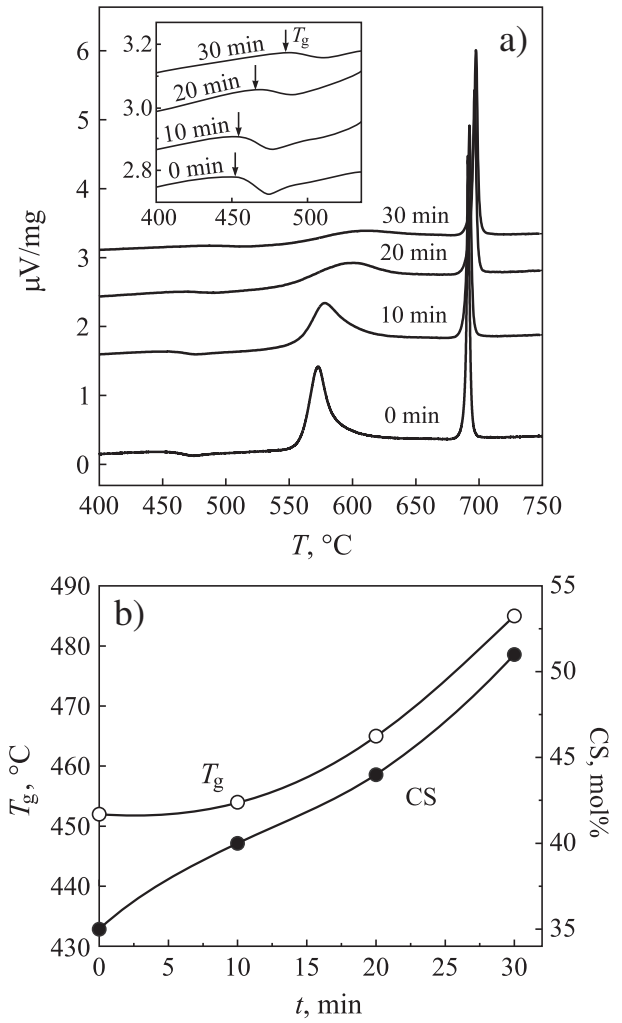

Fig. 17. (a) DSC heating curves of the glass B_{35} and the glass samples heat-treated at $T = 560$ °C for 10, 20, and 30 min. (b) Evolution of the residual glass composition and glass transition temperature during crystallization.

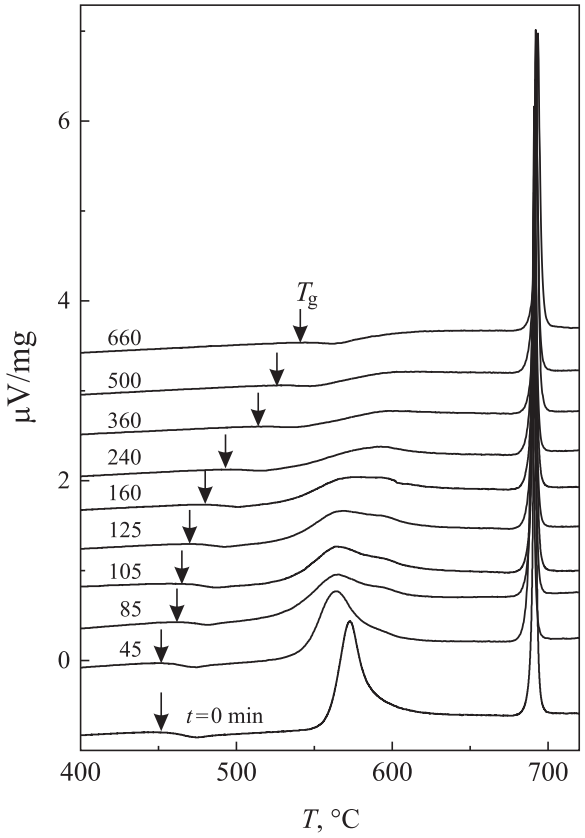

Fig. 18. DSC heating curves of B_{35} glass preliminary partly crystallized at $T = 520$ °C for different periods of time (in minutes) specified close to the respective curves.

to this time, the residual melt contains approximately 40% CS (Fig. 19c). Hence, taking into account the nucleation data (see Fig. 11 in [8]), we expect a decrease of the nucleation rate by 3–4 orders of magnitude. A prolongation of the heat-treatment time up to 660 min results in an increase in the CS content of the residual melt up to 67 mol%.

The first exothermic peak in the DSC heating curves shown in Fig. 18 and its evolution with increasing preliminary treatment time at $T = 520$ °C deserves further discussion. This peak is determined by the first step of LS crystallization, that is, the crystallization of LS only, which results in an enrichment of the residual melt by Ca. As shown above, this evolution of the residual melt causes a rate decrease and subsequent arrest of LS crystallization during the isothermal or dynamic regimes of heat treatment. In the latter case, which is opposite to nucleation-growth at constant temperature, a change in the residual melt composition and an increase in temperature affect the crystallization process. These two time-dependent factors act on crystallization in different ways: the increase of Ca content in the residual melt inhibits the crystallization kinetics, whereas the increase of temperature during a DSC run accelerates it. The interplay of these two factors can result in a shoulder on the first crystallization peak, as shown in Fig. 18 (curves for $t = 45$, 85, 105, 125, 160 min). The first preliminary heat-treatment ($t = 45$ min) shifts the first peak position to lower temperatures due to the increase in the crystal number density relative to the parent glass (compare curves for $t = 0$ and 45 min).

As previously noted, the prolongation of the preliminary heat-treatment time at $T = 520$ °C results in an increased crystal phase volume fraction. This increase is due mainly to slow crystal growth, whereas nucleation fully stops at $t \sim 100$ min. Preliminary crystallization decreases the volume of the residual melt and changes its composition, and the area of the first peak of the DSC curve decreases. The peak profile changes in such a way that its maximum shifts to higher temperatures due to the drop in the low temperature part of the curve.

Figs. 16 and 19 show the overall crystallization kinetics restricted to approximately 40–50 vol.% LS crystals, and hence, they present only the slowing down but not the full arrest of the crystallization process, in contrast to the data for glass B_{47}. To extend the volume fraction of LS crystals, we performed a DSC experiment similar to that shown in Fig. 14. The DSC curves (b) in Fig. 20 differ from the heating curve (a) of parent glass B_{35} in the termination of heating after the first exothermic peak caused by LS crystallization (b_1), followed by cooling to $T = 380$ °C (b_2) and then by heating to full crystallization (b_3). As previously discussed, the temperature range between the two exothermic peaks corresponds to the inhibition of LS crystallization prior to the appearance of CS crystals. According to curve (b_3) (see inset), the glass transition temperature of the residual glass is here 594 °C. This value corresponds to a residual liquid composition of approximately 75 mol% CS. This composition is notably very similar to that of the residual melt of glass B_{47} (see Fig. 8).

4. Diffusion zones

As we have demonstrated above, the crystallization of only one of two possible crystalline phases (expected according to the equilibrium phase diagram below the solidus) results in a change in the residual liquid composition. For the analysis of the low temperature crystallization

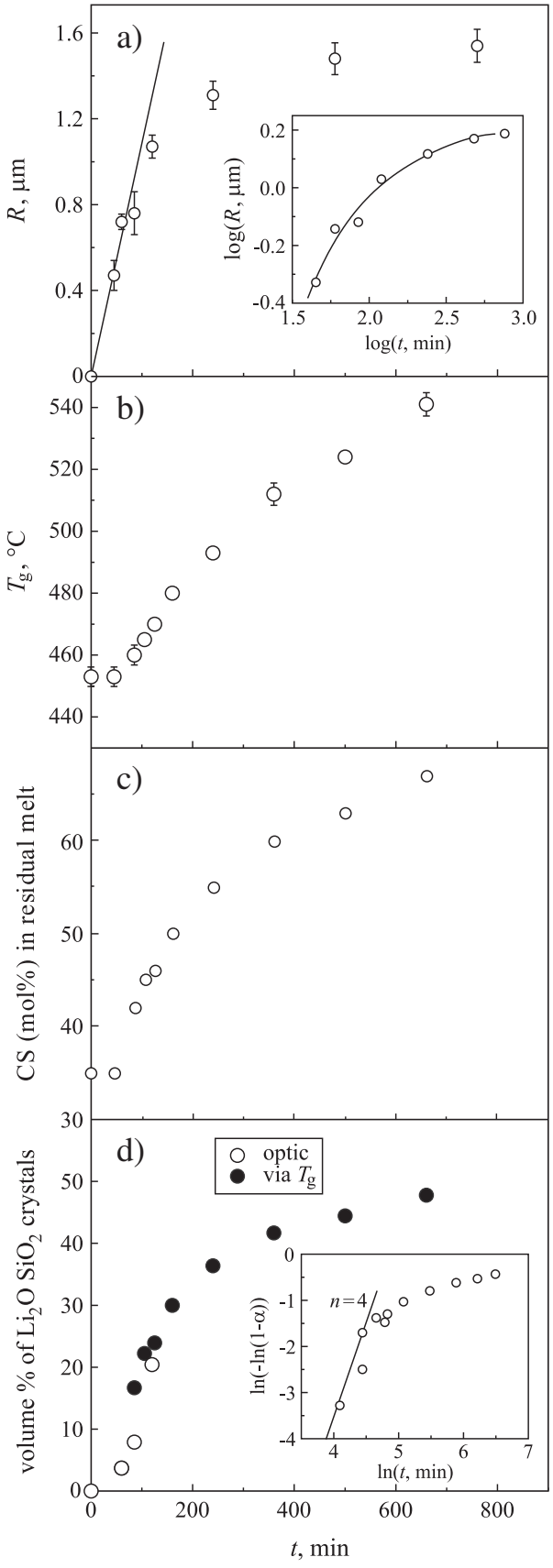

Fig. 19. Dependencies for B_{35} glass on heat-treatment time at $T = 520$ °C of the crystal radius (a), the glass transition temperature (b), composition of residual melt (c), and the volume of crystalline phase (LS) (d).

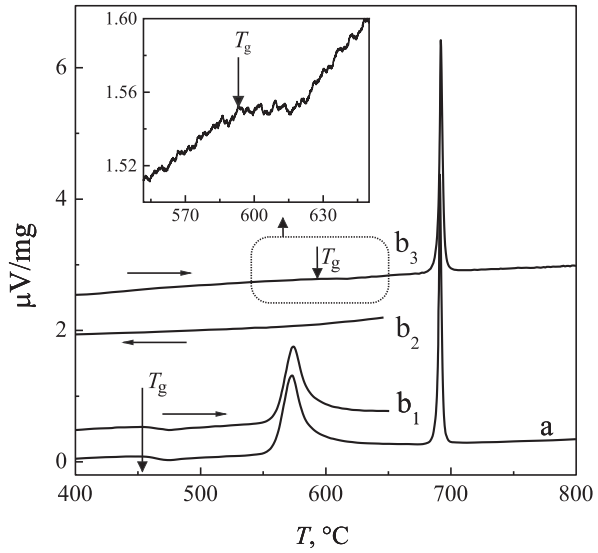

Fig. 20. DSC curves for B_{35} glass. (a) Single heating curve; (b) multistage curves: (b_1) heating up to 650 °C, (b_2) cooling down to 380 °C, (b_3) heating up to full crystallization.

kinetics and especially its two-stage character, it is important to realize that the residual glass composition estimated via its glass transition temperature refers to a glass composition close to the average. As a result, the composition of the residual glass estimated via the DSC-T_g method does not reflect the diffusion zones that form near the crystal–liquid interfaces. These diffusion zones develop and are significant for the crystallization kinetics, especially at the advanced stage of the phase transformation. As discussed below, in the advanced stages of the process, even switching of the occurrence of the different phases (LS–CS–LS) can be found in the diffusion zones near the crystalline phase.

The composition of the diffusion zones can differ significantly from the average melt composition. Fig. 21 shows BSE SEM images of cross sections of B_{47} glass samples heat-treated at 470 °C for 45 h for LS crystal nucleation and then at 675 °C for different periods of time. BSE reveals diffusion zones enriched in Ca (bright area close to the LS crystals) that expand and overlap with increasing growth time. A general depletion in Li (and enrichment in Ca) can be observed as well (compare images (a) and (d)).

The diffusion zones can also be visualized by the spatial intensities of the nucleation-growth process; in the present case, the nucleation rate is extremely sensitive to the variation in glass composition [8]. Fig. 22 shows reflected light-optical micrographs of cross sections of two samples of glass B_{35} (a and b) subjected to a 3-step heat-treatment. In the first step, a constant temperature of $T = 560$ °C is sustained for (a) 10 and (b) 20 min to reveal the LS nuclei that are formed during glass preparation and sample heating to that temperature. In the next step, the samples are sustained at $T = 470$ °C for 3 h to form new nuclei. Finally, the sample is again brought to a temperature $T = 560$ °C and held there for 2.5 min to reveal the nuclei formed in the preceding nucleation step. The micrographs reveal crystals of two different sizes; the larger ones begin growing during the first step of heat-treatment, while the smaller ones only grow during the third step. New crystals do not appear in the vicinity of the larger crystals; they form only in regions far from these crystals (Fig. 22a). Thus, the nucleation kinetics reflects the decrease in Li concentration in the diffusion zones. The shift of glass composition towards CS (reduction of Li) leads to the decrease of the thermodynamic driving force for crystallization due to the drop of liquidus temperature T_L, and hence undercooling (T–T_L), and an increase in nucleus/liquid interfacial energy [8].

According to our estimates of the crystal number density far from the large crystals (see the space marked by a white frame in Fig. 22a), the nucleation rate in this region is approximately 20 times smaller

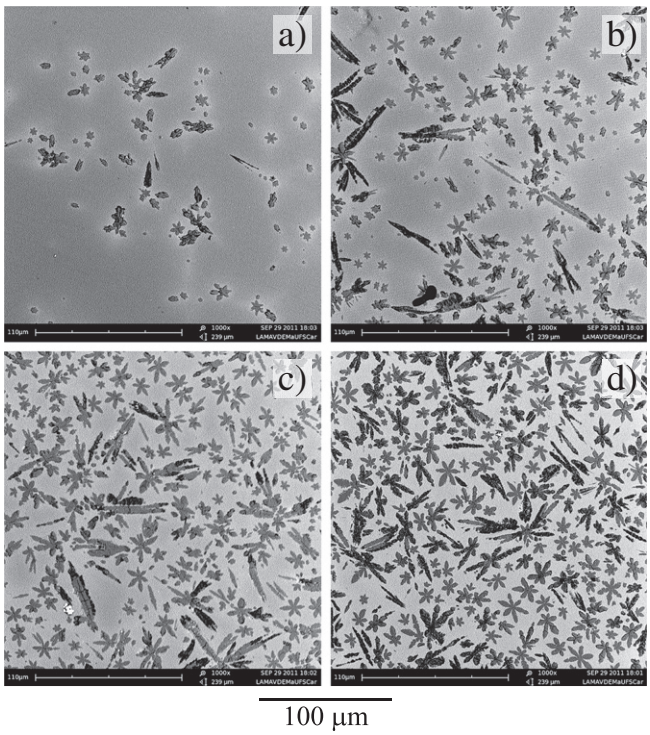

Fig. 21. SEM BSE images of B_{47} glass samples heat-treated at T_n = 470 °C for 45 h and then at T_{gr} = 675 °C for 1 (a), 1.5 (b), 2 (c), and 7 (d) min.

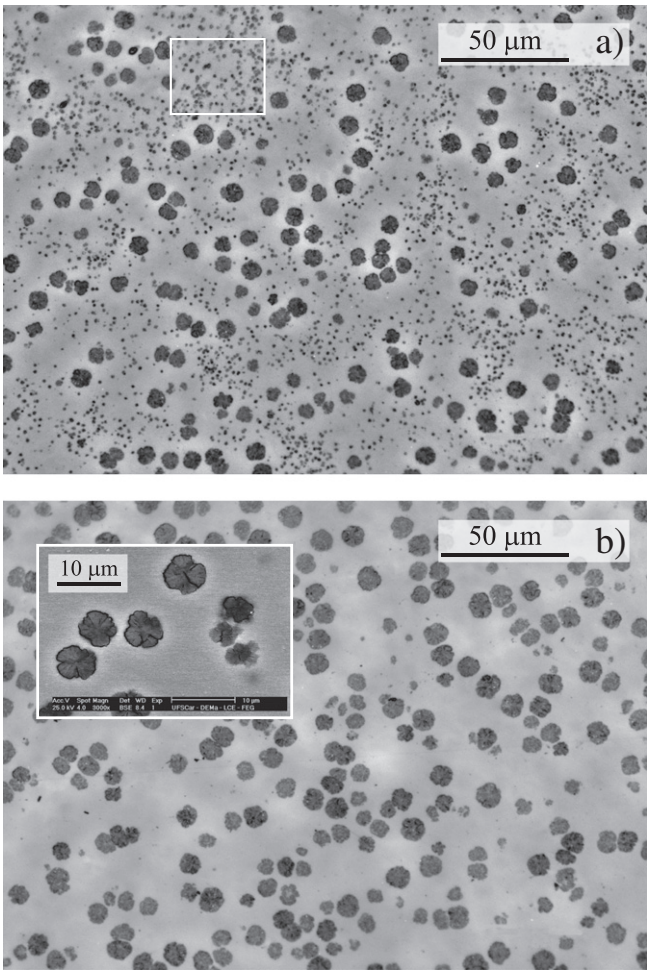

Fig. 22. Reflected light-optical micrographs of B_{35} glass samples subjected to the following triple heat-treatments: a) 560 °C/10 min + 470 °C/3 h + 560 °C/2.5 min b) 560 °C/20 min + 470 °C/3 h + 560 °C/2.5 min. The inset of Fig. 22b presents a SEM BSE image of the same sample.

than that in the original glass B_{35}. Such a nucleation rate could be expected in a glass containing 37–38 mol% CS. Despite the approximations made for this estimate, this composition is close to that estimated via the measurement of T_g (see Fig. 17b). Prolongation of the first heat-treatment time from 10 to 20 min results in full arrest of nucleation in the residual liquid, at least for the same nucleation temperature/time conditions (see Fig. 22b). Indeed, according to Fig. 17b, the average composition of the residual melt after crystallization at 560 °C for 20 min is approximately 56LS44CS (mol%). Based on nucleation data [8], the nucleation rate in this glass at 470 °C is expected to be approximately $2 \cdot 10^9$ m^{-3} s^{-1}. The estimated number density of crystals nucleated at this rate for 3 h is approximately $2 \cdot 10^{13}$ m^{-3}. In the area of the full cross section surface shown in Fig. 22b, this number of crystals would result in approximately one crystal track, so new crystals really cannot be detected. The inset in Fig. 22b presents an SEM BSE image of the same sample, revealing a diffusion zone around the crystals. We thus conclude that, at the given conditions (T = 560 °C/10 or 20 min), detectable depletion of Li occurs for the whole residual liquid.

As demonstrated above, in the case of both eutectic glass (B_{47}) and glass with a composition far from eutectic (B_{35}), the residual melt in which growth of LS crystals is strongly suppressed or fully arrested has a composition of approximately 70–75 mol% CS. Now we shift our attention to two glasses located to the right of the eutectic composition (B_{66} and B_{60}), for the purpose of better understanding the crystallization of glasses with compositions close to that of the residual liquid at advanced stages of crystallization. Bulk nucleation was notably not detected for these two glasses.

Fig. 23 presents an SEM BSE image of a cross section perpendicular to the external surface of a B_{66} glass sample treated at T = 675 °C for 12 min. The crystallized surface layer consists mainly of CS crystals separated by thin layers of LS crystals. SEM BSE reveals chemical contrast, so CS and LS crystals can be distinguished by bright and dark colors, respectively. Despite the fact that the crystalline surface layer of B_{47} glass consists of LS crystals alternating with a residual melt enriched in Ca, the total composition of the surface layer – in the cases of both glasses B_{47} and B_{66} – should coincide with that of the corresponding parent glasses. Therefore, the melt composition of the internal part of the sample does not change.

Pronounced diffusion zones bordering the crystalline surface-melt interface is revealed by the SEM BSE image shown in Fig. 24a. The upper surface layer of glass B_{66} consists mainly of CS crystals; thus, this diffusion zone is enriched by lithium (light element), and its color is darker than that of the melt far from the interface. The diffusion zone bordering the LS crystals in glass B_{47} is enriched by Ca and has a bright color (compare Fig. 24a, b and c).

As shown in Fig. 25, small LS crystals form in glass B_{66} at the CS crystal-melt interface, which is a Li-rich zone. Inside this diffusion zone, these crystals generate their own Li-depleted diffusion zones, which are marked in Fig. 25 by arrows. Thus, two different types of diffusion zones can be simultaneously observed.

The combined formation of two different phases (CS and LS) in glass B_{66}, which is similar to the crystallization of glass B_{60} (see Fig. 26), resembles the alternation of phases at eutectic crystallization and most likely reflects the final stage of residual melt crystallization in glasses B_{47} and B_{35}. Crystallization of different phases mainly occurs in proper thin diffusion zones; therefore, the composition of the residual liquid far from the crystallization front does not change or changes only weakly. Such a scenario can explain the constant glass transition temperature observed at the advanced stage of simultaneous crystallization of LS and CS crystals (see Fig. 9).

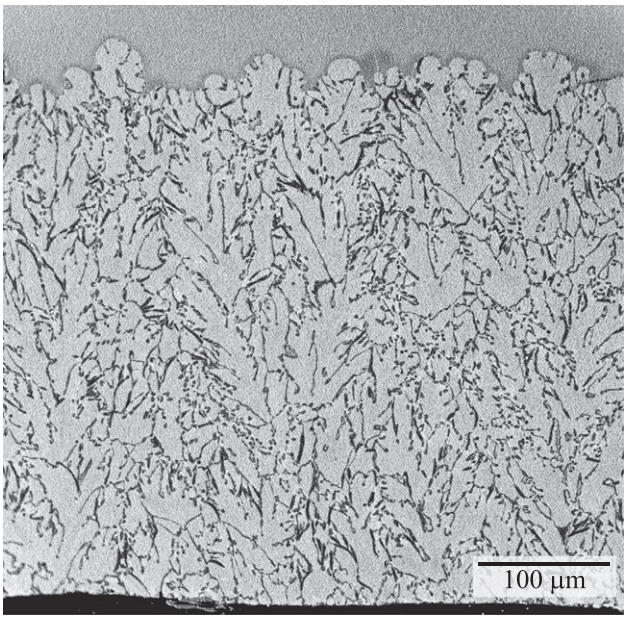

Fig. 23. SEM BSE image of the cross sections of the sample of glass B_{66} perpendicular to their external surface. The sample were heat-treated at $T = 675$ °C for 12 min.

5. Discussion

The results outlined in the present paper demonstrate that the kinetics of overall crystallization of LS–CS glasses proceeds in a two-stage process that is characterized by initial formation of only one of the crystalline phases (LS); the rate of its formation temporarily decreases and then terminates, until it is renewed due to the formation of CS crystals and the resulting from latter process changes in the melt composition.

In order to explain this feature in more detail, we start the discussion from the phase diagram shown in Fig. 1. This figure represents an equilibrium phase diagram that only shows the stable states of the system.

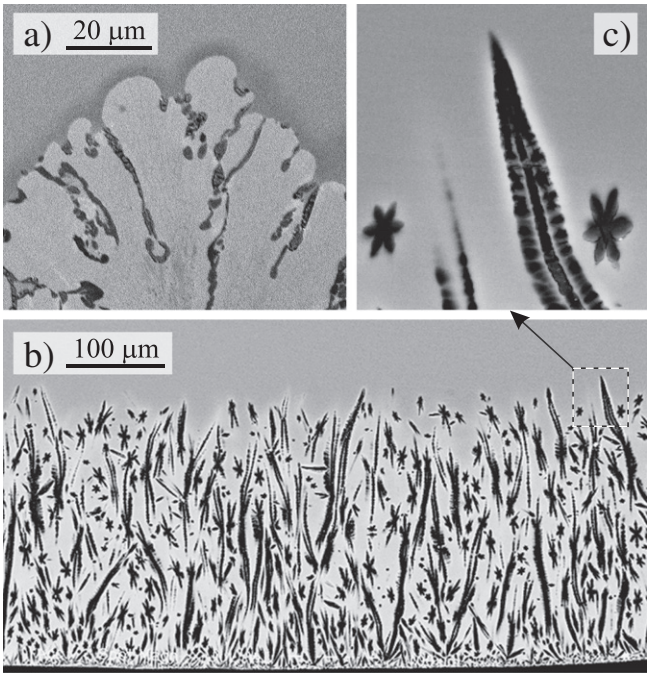

Fig. 24. SEM BSE images of the cross sections of the samples of glasses B_{66} (a) and B_{47} (b, c) perpendicular to their external surfaces. The samples were heat-treated at $T = 675$ °C for 12 (a), and 5 (b, c) minutes.

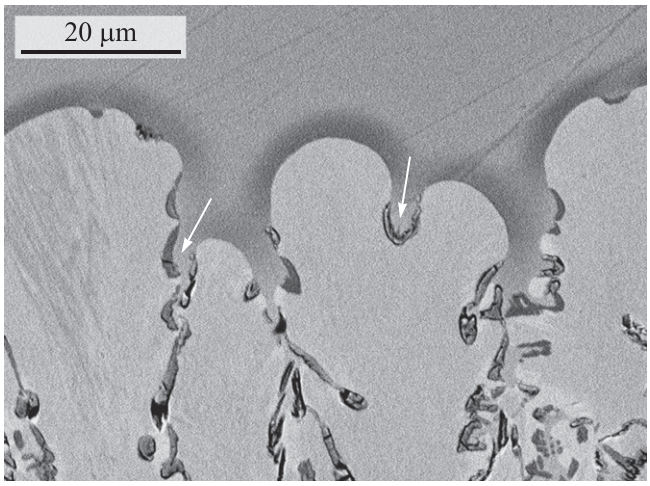

Fig. 25. SEM BSE image of the cross section perpendicular to the external surface of the B_{66} glass sample heat-treated at $T = 700$ °C for 10 minutes.

According to this diagram, two crystalline phases (LS and CS) must eventually form at temperatures lower than the solidus temperature, T_S. However, in the previously discussed process of crystallization of glasses B_{35}, B_{47} and B_{50} at temperatures far from T_S over relatively long periods of time, the overall crystallization is exclusively determined by nucleation and growth of LS crystals. CS crystallization is kinetically suppressed by the poor mobility of Ca ions as compared to that of the Li ions. The overall crystallization of only one phase (LS) results in the progressive shift of the residual liquid composition towards calcium metasilicate (see Section 3).

In the absence of CS crystals, the establishment of a temporary equilibrium between LS crystals and liquid is thermodynamically possible and achieved. This state is defined by the condition of equality of the chemical potentials of the structural unit (Li_2OSiO_2) in the liquid to those in the crystalline phase. This situation is schematically illustrated in Fig. 27, in which the Gibbs free energies of LS (G^{LS}) and CS (G^{CS}) crystals and the liquid (G^{li} (x_{LS})) for a given temperature are plotted versus the composition of the liquid, x_{LS},where x_{LS} is the molar fraction of LS. The composition of the parent liquid is specified as $x_{LS}^{p/l.}$ The particular value x_{LS}^{*} corresponds to the composition of the liquid that is in equilibrium with the LS crystal phase because the tangent to the $G^{liq}(x_{LS})$ curve at x_{LS}^{*} passes through G^{LS}. If the composition of the residual liquid reaches x_{LS}^{*} during the crystallization of LS (see arrows in Fig. 27), the thermodynamic driving force ΔG_V for LS crystallization becomes equal

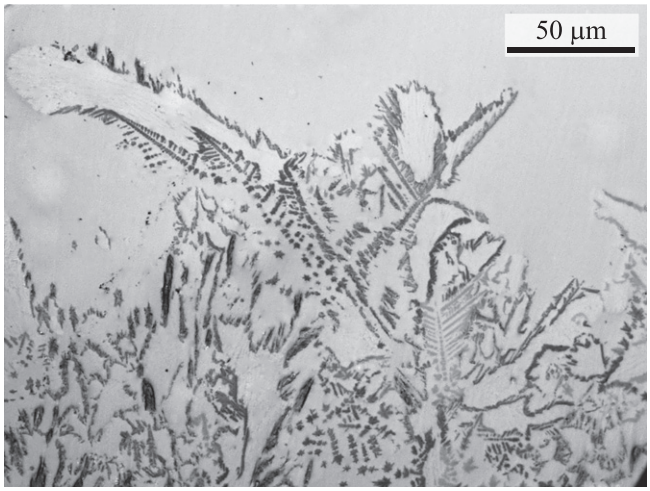

Fig. 26. Reflected light-optical micrograph of the cross section perpendicular to the external surface of the B_{60} glass sample heat-treated at $T = 657$ °C for 15 min.

to zero, and the phase transformation stops. In fact, this case corresponds to a prolongation of the liquidus of the left side of the equilibrium diagram beyond the eutectic composition, as shown in Fig. 28; in other words, a metastable liquidus has been reached (see, for example, also [12,13]). The composition of the residual liquid, at which the growth of LS crystals at $T = 675$ °C stops, can be estimated (using the T_g of the residual melt) to be approximately 75 mol%; it is marked in the figure by a star. According to the above interpretation of the two stage kinetics of LS crystallization, this point must belong to the liquidus line of the metastable phase diagram. According to Eq. (5),

$$\Delta G_V = (T_L - T)(\Delta S_m - R \ln x_{LS})/V_m \quad (5)$$

the thermodynamic driving force of LS crystallization, ΔG_V, approaches zero as the value of T_L approaches the given crystallization temperature T, due to evolution of the composition of the residual liquid. In Eq. (5), ΔS_m is the entropy of fusion per mole of pure crystal, and V_m is the molar volume. This relationship was derived in [14] and has been employed by us already in [8] for the analysis of the nucleation rates of the LS crystal phase.

A prolongation of the *liquidus* curve, shown by the dashed line in Fig. 28, was performed via Eq. (7):

$$T_L(x_{LS}) = T_m[1 - (R/\Delta S_m)\ln x_{LS}]^{-1}[1 + \alpha_l(x_{LS})/\Delta H_m], \quad (7)$$

where ΔH_m is the enthalpy of fusion per mole of pure crystal, and $\alpha_l(x_{LS})$ was used as a fit parameter,

$$\alpha_l(x_{LS})/\Delta H_m = -\left(0.028(1-x_{LS})^2 + 0.41(1-x_{LS})^4\right). \quad (8)$$

The composition of the residual liquid at which the growth of LS crystals stops (marked by a star) is close to the calculated *liquidus* line. This coincidence gives indirect support to our proposed explanation of the origin of the temporary termination of LS crystallization. However, for a more precise specification of the metastable *liquidus*, experimental data on the LS crystallization kinetics at lower temperatures are required. Moreover, the decrease of Li mobility due to the evolution of the composition of the residual liquid can also affect the growth of LS crystals. However, this effect, eventually of major importance at deep undercooling, is negligible compared to the inhibition of growth caused by the decrease of the thermodynamic driving force for crystallization as the latter approaches zero, that is, when T_L of the residual liquid approaches the crystallization temperature T. The pathway of the phase transformation described here is possible only when CS is kinetically unavailable for crystallization. The formation of CS crystals immediately makes the equilibrium between LS crystals and liquid unstable because it causes changes in the melt composition. Deviations of the actual composition of the melt from the metastable equilibrium composition x_{LS}^* allow, in addition to the formation of CS-crystals, also the further formation and growth of the LS-phase. Such two-stage kinetics of the overall crystallization of crystal phases, similar to that described in the present paper, could be expected to govern the evolution of the crystallization kinetics of systems with sufficiently high differences in the mobilities of their structural elements that participate in the formation of different crystalline phases.

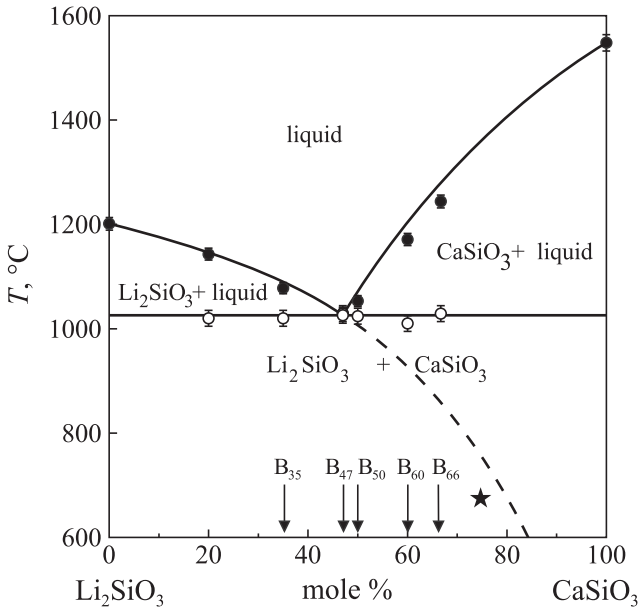

Fig. 28. Phase diagram of the pseudo-binary joint Li_2SiO_3 – $CaSiO_3$. The dashed line is the calculated metastable liquidus (see text). Star corresponds to the residual melt composition in B_{47} glass sample crystallized at $T = 675$ °C (see Fig. 9).

To further advance the above given description of the crystallization kinetics in the system under consideration, a number of further topics could be addressed in future. In particular, in cases when the induction period preceding the formation of CS-crystals is determined by the time-lag for nucleation, there must be a strong temperature dependence in the kind of crystallization behavior. Consequently, a detailed analysis of how the scenario of the crystallization process may eventually change with variations of temperature would be highly interesting. Such analysis could also help to refine the proposed metastable liquidus curve. Moreover, the knowledge of the concentration dependence of Ca and Li partial diffusion coefficients is very important for the analysis of crystallization kinetics. Its account could give a more refined description of the process and is also worth of further detailed investigation.

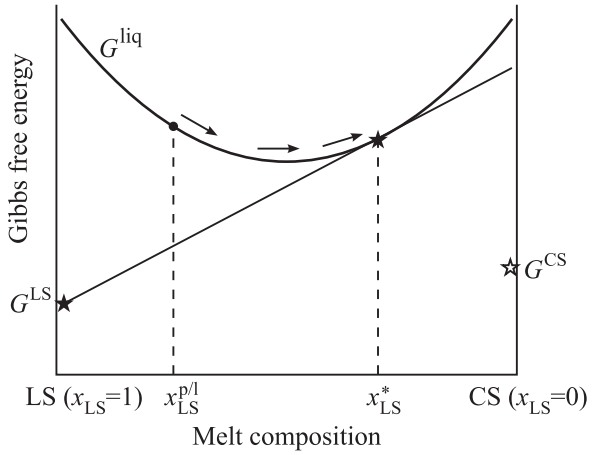

Fig. 27. Schema of the Gibbs free energies of LS (G^{LS}) and CS (G^{CS}) crystals and liquid (G^{li} (x_{LS})) versus their composition. x_{LS} is the molar fraction of LS.

6. Conclusions

Significant differences in the mobilities of Li and Ca ions, which determine the growth of lithium and calcium metasilicates, result in a notable delay of CS formation as compared to LS formation in glasses of the LS-CS joint. Consequently, in the initial stages of crystallization, only the formation of LS is observed. In this stage, the overall crystallization of LS shifts the composition of the residual melt towards calcium metasilicate and is *terminated* when the latter approaches the composition corresponding to the metastable *liquidus* (LS crystal-melt) at the given temperature. LS crystals then remain in equilibrium with the

residual melt until CS crystals form (by heterogeneous nucleation and growth), which immediately makes such equilibrium unstable. The growth of CS leads to changes in the composition of the residual liquid, resulting in a shift of the melt composition and, consequently, in the *resumption* of LS crystallization and eventually full crystallization. This pathway of crystallization kinetics can be expected to generally occur for non-stoichiometric systems with sufficiently high differences in the mobilities of their structural elements, which determine the crystallization kinetics of different crystalline phases. These findings may be useful for the compositional design of complex, multicomponent glass–ceramics.

Acknowledgments

We are thankful to the Brazilian funding agencies CNPq, grant # 2012/17417-9 and CEPID grant # 2013/07793-6, São Paulo Research Foundation (FAPESP) for generous funding of this research.

References

[1] G.P. Souza, V.M. Fokin, E.D. Zanotto, J. Lumeau, L. Glebova, L.B. Glebov, Phys. Chem. Glasses: Eur. J. Glass Sci. Technol. 50 (2009) 311.
[2] G.P. Souza, V.M. Fokin, E.D. Zanotto, J. Lumeau, L. Glebova, L.B. Glebov, J. Am. Ceram. Soc. 93 (2010) 716.
[3] R.P. Fogaça de Almeida, C. Bocker, C. Rüssel, Chem. Mater. 20 (2008) 5916.
[4] T. Berthier, V.M. Fokin, E.D. Zanotto, J. Non-Cryst. Solids 354 (2008) 1721.
[5] J.W.P. Schmelzer, H. Ulbricht, J. Colloid Interface Sci. 117 (1987) 325.
[6] J.W.P. Schmelzer, A.S. Abyzov, J. Chem. Phys. 134 (2011) 054511.
[7] J.W.P. Schmelzer, A.S. Abyzov, Comments on the thermodynamic analysis of nucleation in confined space, J. Non-Cryst. Solids (2013), http://dx.doi.org/10.1016/j.jnoncrysol.2013.04.024.
[8] V.M. Fokin, R.M.C.V. Reis, A.S. Abyzov, C.R. Chinaglia, E.D. Zanotto, J. Non-Cryst. Solids 362 (2013) 56.
[9] A.R. West, J. Am. Ceram. Soc. 61 (1978) 152–155.
[10] V.M. Fokin, A.A. Cabral, R.M.C.V. Reis, M.L.F. Nascimento, E.D. Zanotto, J. Non-Cryst. Solids 356 (2010) 358.
[11] M. Avrami, J. Chem. Phys. 7 (1939) 1103, (8 (1940) 212; 9 (1941) 177).
[12] V.Ya. Anosov, M.I. Ozerova, Yu.Ya. Fialkov, Osnovy fiziko-khimicheskogo analiza (Foundations of the Physicochemical Analysis), Moscow, Nauka, 1975. , (in Russian).
[13] I.A. Aksaf, J.A. Pask, J. Am. Ceram. Soc. 58 (1975) 507.
[14] C.V. Thompson, F. Spaepen, Acta Metall. 31 (1983) 2021.